

# Vision-Based Adaptive Robotics for Autonomous Surface Crack Repair

Joshua Genova<sup>a</sup>, Eric Cabrera<sup>b</sup>, Vedhus Hoskere<sup>a,c,\*</sup>

<sup>a</sup> Department of Electrical and Computer Engineering, University of Houston, 4226 MLK Blvd, Houston, TX 77204, United States

<sup>b</sup> Department of Mechanical Engineering, University of Houston, 4226 MLK Blvd, Houston, TX 77204, United States

<sup>c</sup> Department of Civil and Environmental Engineering, University of Houston, 4226 MLK Blvd, Houston, TX 77204, United States

\* Corresponding author at: Department of Civil and Environmental Engineering, University of Houston, 4226 MLK Blvd, Houston, TX 77204, United States

E-mail addresses: [jtgenova@cougarnet.uh.edu](mailto:jtgenova@cougarnet.uh.edu) (J. Genova), [vhoskere@central.uh.edu](mailto:vhoskere@central.uh.edu) (V. Hoskere).

## Abstract

Surface cracks in infrastructure can lead to significant deterioration and costly maintenance if not efficiently repaired. Manual repair methods are labor-intensive, time-consuming, and imprecise and thus difficult to scale to large areas. Breakthroughs in robotic perception and manipulation have advanced autonomous crack repair, but proposed methods lack end-to-end testing and adaptability to changing crack size. This paper presents an adaptive, autonomous system for surface crack detection and repair using robotics with advanced sensing technologies. The system uses an RGB-D camera for crack detection, a laser scanner for precise measurement, and an extruder and pump for material deposition. A novel validation procedure with 3D-printed crack specimens simulates real-world cracks and ensures testing repeatability. Our study shows that an adaptive system for crack filling is more efficient and effective than a fixed-speed approach, with experimental results confirming precision and consistency. This research paves the way for versatile, reliable robotic infrastructure maintenance.

*Keywords:*

Robotics

Infrastructure maintenance

Crack repair

Adaptive repair

End-effector design

Automation

Computer vision

## 1. Introduction

In the field of infrastructure maintenance, the efficient detection and repair of surface cracks represents one of the most persistent and challenging problems. Surface cracks are typically non-structural but can lead to long-term deterioration due to moisture or chemical ingress. Over time, these minor imperfections may propagate and become structurally significant, potentially leading to costly repairs or even catastrophic failures. For example, from 2016 to 2018, surface crack repair in San Francisco International Airport runways cost close to half a million dollars directly, and millions more in economic impact due to the 1,103 flights that were cancelled, and 13,217 flights were delayed during repair days [1]. These statistics emphasize the noteworthy benefits that could be unlocked by timely, efficient, and proactive surface crack detection and repair that prevent such economic losses and disruptions. Additionally, in the aftermath of earthquakes such as the 2011 Christchurch earthquake, inspection and repair efforts can take weeks, months, or even years due to a lack of manpower and inaccessibility [2,3]. Implementing autonomous systems for repair can provide immediate relief by drastically reducing the time required for repairs and minimizing associated risks. Moreover, the presence of surface cracks is aesthetically displeasing and may reduce the structure's value. Therefore, surface cracks need to be frequently repaired as part of routine maintenance of infrastructure assets. Fig. 1 shows cracks in an airport runway, a building wall post-earthquake, and

unsightly crack on top of a door. Traditional methods, such as pouring, filling, sealing, pressure pouring, and banded digging-patching [4], rely heavily on manual labor, and are time-consuming and prone to human error. These manual processes often result in inconsistent repair quality and pose major safety risks, especially in hazardous or hard-to-reach areas. In addition, underfilling or overfilling material can lead to premature failure, adhesion problems, material waste, and unsightly repairs. Given these challenges, there is a critical need for innovative solutions. The integration of adaptive automation and robotics offers a promising approach to enhance accuracy, efficiency, and safety in surface crack repair, ultimately improving the longevity and reliability of infrastructure assets and reducing disruptions.



**Fig. 1.** Surface cracks in different environments: an airport runway under repair (left), a building wall post-earthquake (middle), and a crack above a door (right).

Towards autonomous crack filling, researchers have made progress in two directions: (i) robotic perception and (ii) robotic manipulation. Research on robotic perception for crack filling focuses on achieving accurate and precise localization of cracks, utilizing advanced methods for crack detection and measurement [3–23]. On the other hand, robotic manipulation for crack filling involves developing advanced end-effectors, control methods, and path planning to enable precise and efficient application of repair materials to identified cracks [24–36]. Significant strides have been made in both areas, with numerous studies contributing to the development of more effective and autonomous crack repair systems.

Recent advancements in crack detection, sensing, and measurement have introduced a variety of innovative systems aimed at enhancing precision and efficiency. Hoskere discussed an automated inspection framework for civil infrastructure that involves the development of datasets for deep learning, unmanned aerial vehicles (UAVs), data acquisition, application of deep networks for damage identification, and visualization for decision-making, addressing challenges in data extraction, accuracy, and inspection efficiency [5]. Several works have also focused on infrastructure inspection deploying high-resolution sensors and cameras, frequently mounted on UAVs, automated guided vehicles (AGVs), or robotic manipulators [6–12]. Additionally, many researchers have concentrated on computer vision and deep learning approaches for the detection and segmentation of cracks [13–16]. Multi-sensor systems, utilizing combinations of RGB-D cameras, CNNs, laser scanners, and LiDAR, have achieved impressive accuracy in detecting hairline and sub-millimeter precision cracks [17–20]. Image processing enhancements have further improved depth data and crack detection accuracy, and data fusion approaches have enhanced resolution [21–23]. Similarly, Sheta et al. demonstrated low-cost solutions like the mBot [24] integrated with CNN and phone cameras highlight scalability potential [25]. Collectively, these studies represent breakthroughs in integrating advanced sensors, image processing, and data fusion techniques to enhance precision and efficiency in crack detection technologies.

In the realm of robot manipulation, control, and path planning, several approaches have been explored to enhance autonomous crack repair. Robotics technology is being increasingly leveraged to improve the efficiency and precision of manual repair tasks in various infrastructure maintenance [26,27]. Chen et al. developed a semi-autonomous vision-guided system for crack filling [28]. Zhu et al. also designed a

manipulator that is adaptable to depth variability showing promise in adjusting to various crack conditions [29]. Notable advancements have been made in tracking control accuracy using visual data and in path planning, where efficient algorithms have optimized navigation for detection robots [30,31]. UAV-based systems, including those with soft continuum arms and 3D asphalt printing capabilities, have expanded the possibilities for accessibility and on-site repairs [32–34]. Advanced end-effector designs integrating multiple sensors for sealant width monitoring and computational models for predicting sealant flow offer faster and cheaper solutions [35–38]. These advancements are driving forward the capabilities of autonomous crack repair systems in terms of manipulation and control.

Despite remarkable progress in robotic perception and manipulation for crack repair, several challenges persist, particularly in the integration of detection and repair functionalities of these methods. Many systems, although precise in simulated environments, lack extensive real-world testing and validation, particularly in dynamic and practical conditions such as changing lighting and filler rheology. Existing literature primarily focuses on isolated aspects of the repair process without integrating or validating these components into a cohesive solution as conducting the repair task and objectively evaluating the repair is a challenging problem. Most methods rely purely on visual data and deep learning and computer vision models, but these introduce potential inaccuracies and challenges in varied environments, especially given the high accuracy required for crack repair. Our research aims to synthesize the strengths of these individual approaches into a comprehensive, end-to-end, adaptive, and autonomous system.

This paper discusses a novel methodology for crack-repair that addresses both crack detection and repair with high precision. The three novel contributions of our research are:

- i. An autonomous and adaptive crack filling system using a robotic arm and custom end-effector that integrates detection, measurement, and repair.
- ii. Novel computer vision pipeline to combine RGB-D camera for initial detection combined with laser a laser scanner for precision measurements for crack filling.
- iii. A repeatable validation procedure using a 3D printed crack that compares scans before and after filling.

To demonstrate our contributions, we conduct tests in both simulation and in the laboratory environment by constructing the proposed system.

The remainder of this paper is organized as follows: Section 2 presents the proposed methodology, covering calibration, crack coordinates extraction from image to coordinates, coordinates enhancement and crack profile measurement using a laser scanner, and the crack filling process. Section 3 describes the simulation environment and experimental setup, including the overall system design. Section 4 presents the results of using adaptive speed versus constant speed during crack filling. Finally, Section 5 concludes the paper.

## **2. Proposed methodology**

This section outlines our proposed methodology for crack repair. Our methodology consists of four parts (i) extrusion calibration, (ii) crack coordinates extraction, (iii) crack profile, and (iv) crack filling. [Fig. 2](#) illustrated the methodology through a high-level system overview. The proposed methodology begins with a calibration process where material is printed at various speeds and measured to determine extrusion rates. Next, crack coordinates are extracted using an image to segment the crack via a pre-trained model, extracting centerline pixels, and transforming them into robot coordinates. Subsequently, the system refines these coordinates with a laser scanner, enhancing precision and measuring the cross-sectional area to adjust the robot's speed for accurate filling. The crack filling process then begins where material is pumped from a custom-designed, 3D-printed pump to the print head, extruded at a constant flow rate, which is driven by a microprocessor. The robot moves to the coordinates at assigned speeds to ensure precise filling. Finally,

we discuss the proposed validation methodology through a rescan for post-fill profiles, applying heuristic algorithms to detect cross-sectional area, and ensuring the crack is properly repaired.

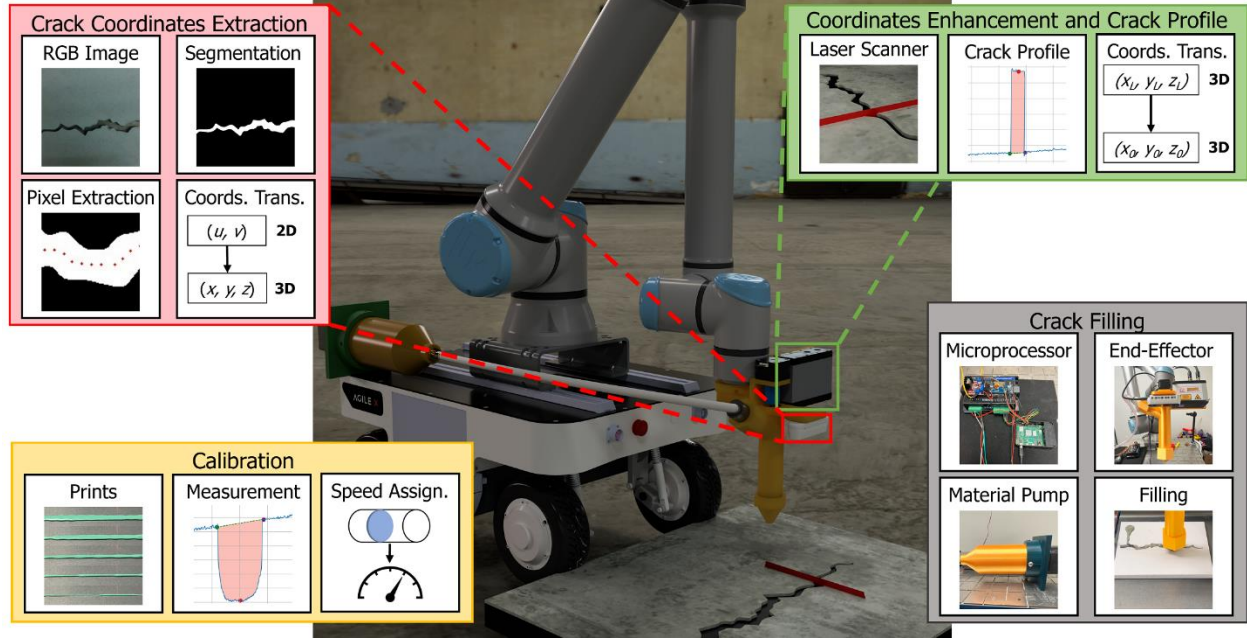


Fig. 2. High-Level System Overview.

## 2.1 Extrusion Calibration

The calibration process is crucial for ensuring accurate material extrusion during crack repair. However, the rheology of the crack filler mixture presents challenges that are not the focus of this project. We strive to maintain consistent mixture properties for every experiment, but variations can occur due to several factors. One challenge is the reuse of the material; since the proportions of clay and water in the reused material are not precisely known, we add more until we achieve an ideal consistency. Additionally, heat and humidity can affect the mixture's properties. To reduce costs, we save and reuse as much material as possible after each experiment. Therefore, the calibration process is essential for determining the extrusion rate at different speeds, ensuring reliable and accurate material deposition. To begin, we print a strip of material at different speeds and measure the cross-sectional area with the laser scanner. The laser scanner provides 2D measurements, with the x-axis representing the width of the scanned line and the y-axis representing the distance from the laser scanner. To calculate the actual width and height of the print, we employ a heuristic algorithm. First, we identify the indices with the largest rate of change, which indicate the edges of the printed material as shown in Eq. (1). A flat profile from the laser scanner data implies a flat surface with no print. The cross-sectional area  $A$  is then calculated by integrating the  $z$  values over the width, as shown in Eq. (2). The center of the profile is found by averaging these indices as depicted in Eq. (3) and Eq. (4). This process ensures precise measurements of the height and cross-sectional area of the printed material, which are essential for accurate material extrusion during the crack repair process.

$$x_1 = \mathbf{x}[i_1]; \quad x_2 = \mathbf{x}[i_2] \quad (1)$$

$$A = \int_{x_1}^{x_2} z dx \approx \sum_{i=i_1}^{i_2} z[i] \Delta x \quad (2)$$

$$i_{avg} = \frac{i_1 + i_2}{2} \quad (3)$$

$$(c_x, c_y) = (x[i_{avg}], z[i_{avg}]) \quad (4)$$

Where  $x_1$  and  $x_2$  are the  $x$  value from the laser scanner data at  $i_1$  and  $i_2$ , the two indices with the largest sudden change of the laser depth  $z$ ,  $A$  is the cross-sectional area,  $\Delta x$  is the change between the  $x$  values,  $i_{avg}$  is the average of the two indices, and  $c_k$  is the center position of the crack in the  $k$  axis.

## 2.2 Crack Coordinates Extraction

After calibration, 3D crack coordinates are extracted to allow for automated navigation of the robot along the length of the crack. The crack coordinate extraction process begins by detecting cracks using a segmentation model applied on RGB images, followed by extracting centerline pixel coordinates through skeletonization. These pixels are then transformed from camera coordinates to robot coordinates using the pin-hole camera model, and the final path is optimized using a heuristic approach. This section details the methods used for detecting cracks and transforming the detected coordinates into format that the robot can interpret and use.

### 2.2.1 Crack Detection using CNN and Stereo Depth Camera

Accurate crack detection is the foundation of our proposed repair process. We start with the assumption that the robot has already been moved so that a crack is visible in the frame of the RGB-D camera. Then, an image is captured, and a crack segmentation algorithm is applied. Our pipeline is agnostic to the specific crack segmentation method utilized. In this paper, we apply a pretrained DeepLabV3+ model, trained on the conglomerate crack dataset containing over 10,000 images [39–44]. The captured RGB image is fed into the DeepLabV3+ model, which segments the crack and outputs a black-and-white image mask highlighting the crack. Fig. 3 illustrates this process: The first row of the figure shows the original RGB image, the second row displays the segmented mask, and the last row demonstrates the overlay of the segmentation on top of the original RGB image. This overlay helps in visually assessing the model's segmentation performance. By integrating the RGB-D camera with the advanced DeepLabV3+ model, we achieve a robust and accurate crack detection system, forming the basis for the subsequent stages of the repair process.

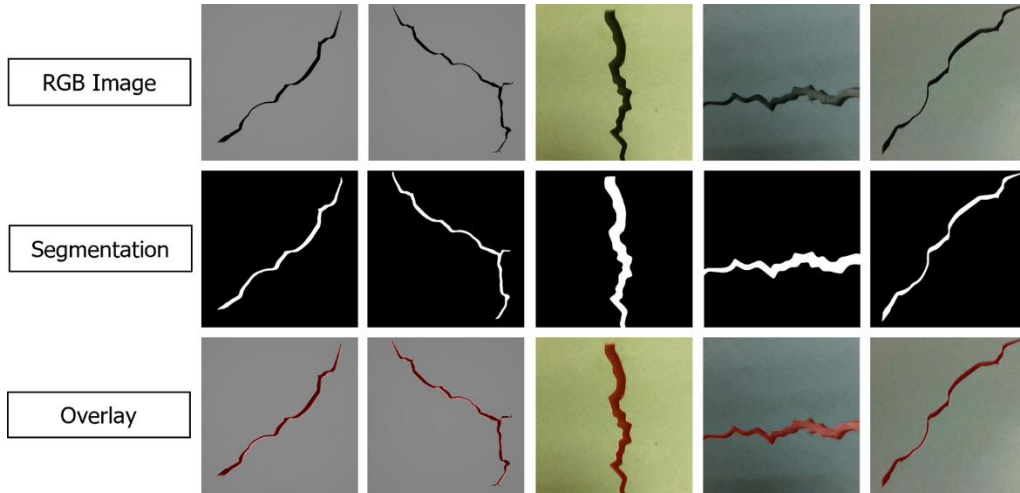


Fig. 3. Image Capture and Segmentation.

### 2.2.2 Image Pixel Extraction

With the mask image from the segmentation model, we proceed to extract the pixel coordinates of the crack as depicted in Fig. 4. First, we convert the segmented mask image to grayscale to simplify the data, ensuring that the crack stands out against the background. We then apply a binary threshold to the grayscale image, creating a clear black-and-white binary image where the crack is distinctly represented. Next, we perform skeletonization on the binary image. Skeletonization is a morphological operation that iteratively removes outer pixels of the crack representation, reducing it to its thinnest form while preserving the overall structure [45]. This operation results in a one-pixel-wide skeleton that accurately traces the central path of the crack, providing a precise and simplified representation for subsequent steps. After skeletonization, we extract the coordinates of the skeleton pixels, representing the exact path of the crack. To manage the data effectively, we simplify the coordinates by filtering out points that are too close to each other based on a predefined threshold. This filtering ensures that the dataset is both accurate and efficient, facilitating easier transformation into 3D coordinates for the robotic system's navigation and repair tasks.

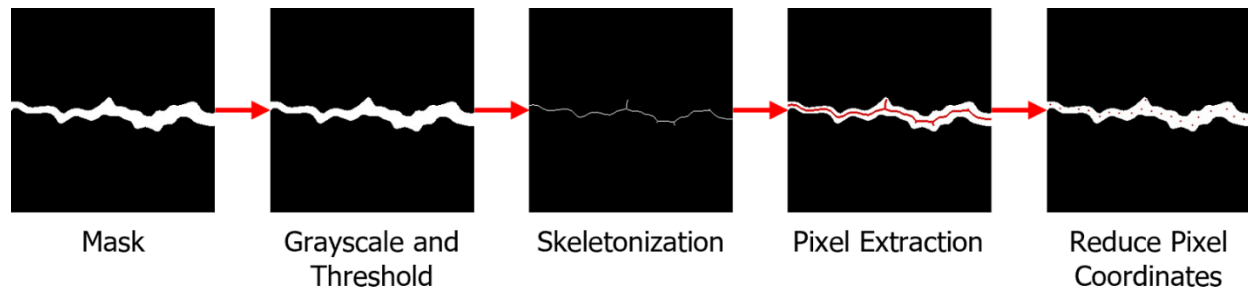


Fig. 4. Pixel Coordinate Extraction Process.

### 2.2.3 Pin-Hole Camera Model

To accurately transform the pixel coordinates of detected cracks into 3D camera coordinates, we use the pin-hole camera model illustrated in Fig. 5. Pin-Hole Camera Model. This model is essential because it translates the 2D image data captured by the RGB-D camera into a spatial format that the robot can use. This transformation allows the robotic system to understand the exact position and orientation of the cracks in the real world, enabling precise and effective repair operations. The pin-hole camera model shows how a point  $\mathbf{P}(X, Y, Z)$  in the 3D world is projected onto the image plane at point  $p$  [46]. The principal point  $(x, y)$  is the projection of the center of the camera onto the image plane, and the distance  $f$  represents the focal length. The center of projection, where all projection lines converge, represents the optical center of the camera. The intrinsic camera parameters are encapsulated in the  $\mathbf{K}$  matrix, as shown in Eq. (5). These parameters include the focal lengths  $(f_x$  and  $f_y)$  and the optical center or principal point  $(p_x, p_y)$ . The intrinsic matrix  $\mathbf{K}$  is critical for accurately mapping the 2D pixel coordinates to 3D space. The transformation from pixel coordinates to camera coordinates is illustrated by Eq. (6), where the Camera Coordinates represent the 3D points in the camera's coordinate system,  $\mathbf{K}$  is the intrinsic matrix, and Pixel Coordinates  $(u, v)$  are the 2D points from the segmented image, with  $z_c$  being the respective depth values obtained from the RGB-D camera.

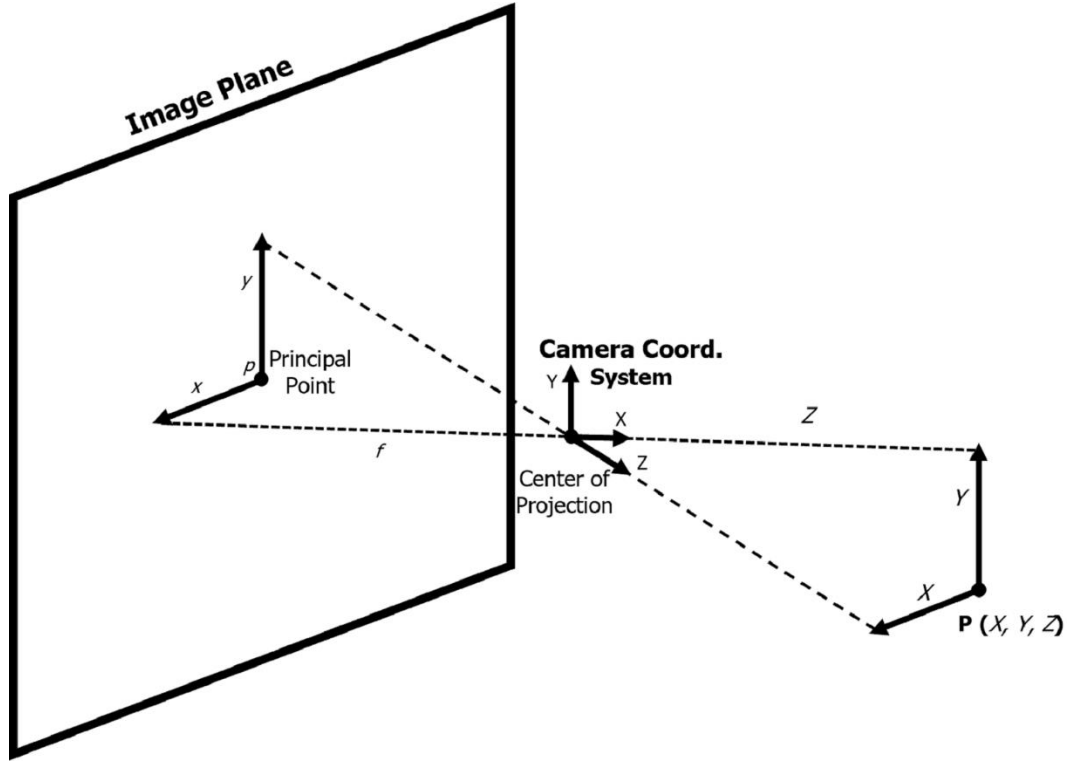


Fig. 5. Pin-Hole Camera Model.

$$K = \begin{bmatrix} f_x & 0 & p_x \\ 0 & f_y & p_y \\ 0 & 0 & 1 \end{bmatrix} \quad (5)$$

$$\begin{bmatrix} x_c \\ y_c \\ z_c \end{bmatrix} = K^{-1} * z_c * \begin{bmatrix} u \\ v \\ 1 \end{bmatrix} \quad (6)$$

#### 2.2.4 Transformation from Camera Coordinates to Robot Coordinates

Robot coordinates are then computed from the camera coordinates. We create a transformation matrix that converts the camera coordinates into the robot base's reference frame using the camera's extrinsic parameters, including its translation and rotation relative to the robot's base using the robot's API. The transformation from camera coordinates to robot base coordinates is defined by Eq. (7), where  $T_0^C$  is the transformation matrix. Fig. 6 illustrates the overall process, from pixel coordinates to robot base coordinates. The origin in the image plane, depicted by  $o_{image}$ , is where the pixel coordinates of the crack are located. The crack coordinates in the image plane are then transformed to camera coordinate system using the approach discussed previously, resulting in a new origin,  $o_{camera}$ . Subsequently,  $o_{camera}$  is transformed into  $o_{robot}$ , which is the origin of the robot base frame, thereby converting the crack coordinates in the camera coordinate system to the robot base coordinate system. By transforming the camera coordinates to robot coordinates, the robotic system can interpret and act upon the spatial positioning of the cracks, ensuring accurate and effective repair operations.

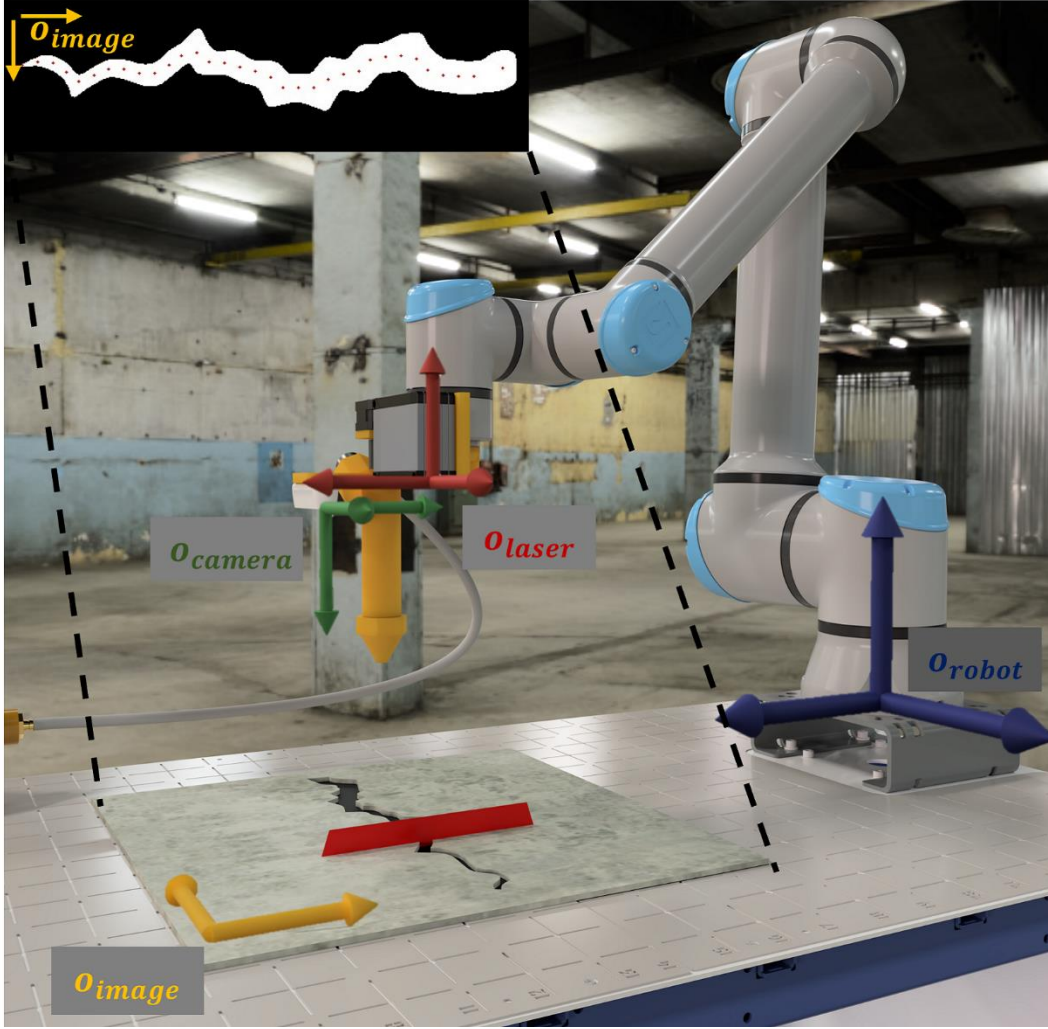


Fig. 6. Transformation from 2D Image Coordinates to 3D Robot Base Coordinates.

$$\begin{bmatrix} x_0 \\ y_0 \\ z_0 \end{bmatrix} = T_C^0 * \begin{bmatrix} x_c \\ y_c \\ z_c \end{bmatrix} \quad (7)$$

### 2.2.5 Path Optimization using Heuristic Approach

Once the crack coordinates have been transformed into the robot's coordinate system, the next step is to optimize the path for the robot to follow during the repair. Using a heuristic approach, we aim to minimize travel distance, ensure complete coverage, and avoid redundant movements. After the image pixel extraction, the robot coordinates are stored in random order. To optimize the path, the algorithm first calculates the maximum distances between the x and y coordinates. Depending on which distance is greater, the coordinates are sorted along either the x or y axis, ensuring efficient navigation along the crack. While other path optimization algorithms, such as the Two-Opt Algorithm, Genetic Algorithm, and Held-Karp Algorithm, were considered, the heuristic approach proved sufficient for the generally horizontal and vertical crack patterns tested in this paper. For more complex patterns, like diagonal or branching cracks, more advanced algorithms may be necessary. By employing this heuristic approach, we enhance the robot's efficiency and precision, reducing time and material usage while maintaining high repair quality.

## 2.3 Coordinates Enhancement and Crack Profile

In this section, we describe the methods used to enhance the initial image-based crack coordinates and generate accurate crack profiles. Due to the RGB-D camera's large depth value error, the converted crack coordinates may lack accuracy, making enhanced coordinates essential for precise robot navigation. Accurate crack profiles are also vital for determining the cross-sectional area at each coordinate, which in turn helps to identify the appropriate speed needed for optimal material extrusion.

### 2.3.1 Laser Scanning, Data Acquisition, and Profile Generation

To enhance the accuracy of the initially detected crack coordinates, we use a laser scanner to capture high-resolution data along the crack. The laser scanner projects a line of laser light onto the surface and captures the reflected light to measure the distance accurately, generating detailed 2D profiles at regular intervals. The same heuristic algorithm is used from the calibration process to generate the profile of the crack. The main difference is instead of height of the print, we have the depth of the crack. The result is a cross-sectional profile of the crack, which is necessary for planning the material deposition during the repair process. By generating accurate crack profiles, we can correlate which robot speed is needed at specific crack coordinates to properly fill the crack at that point.

### 2.3.2 Transformation from Laser Coordinates to Robot Coordinates

The crack coordinates from the laser scanner coordinate systems are then transformed to the robot coordinate system. The center point of the crack in laser coordinates is obtained from the profile using the algorithm described in Eq. (4). The center x-coordinate,  $c_x$  shows how far the original point is from the true center of the crack on its x-axis, or y-axis depending on the crack pattern, with a value of 0 indicating the exact center. The center y-coordinate,  $c_y$  from represents the distance of the laser scanner from the center of the crack on its z-axis. Depending on the crack pattern, Eq. (8) for horizontal crack, and Eq. (9) for vertical cracks. This information is used to correct the previous robot coordinates using Eq. (10), transforming into the robot base's reference frame using a transformation matrix,  $T_L^0$ . This matrix, derived from the laser scanner's translation and rotation parameters obtained via the robot's API, is applied to the center coordinates to transform them into the robot base coordinates. Fig. 6 illustrates the transformation from the laser coordinate system origin  $o_{laser}$  to the robot base coordinate system  $o_{robot}$ .

$$\text{Horizontal Cracks} \begin{cases} x_L = c_x \\ y_L = 0 \\ z_L = c_y \end{cases} \quad (8)$$

$$\text{Vertical Cracks} \begin{cases} x_L = 0 \\ y_L = c_x \\ z_L = c_y \end{cases} \quad (9)$$

$$\begin{bmatrix} x_0 \\ y_0 \\ z_0 \end{bmatrix} = T_L^0 * \begin{bmatrix} x_L \\ y_L \\ z_L \end{bmatrix} \quad (10)$$

## 2.4 Crack Filling

With the accurate crack coordinates and profile, the robot can begin filling the crack. The filling material is pumped through a custom-designed pump to the end-effector, which features a print head that extrudes the filling material. In a similar manner to traditional 3D printing technology using Polylactic acid (PLA), some material is initially extruded at the start of the repair process to ensure a consistent flow and to clear any potential blockages in the nozzle. This initial extrusion helps to minimize any inconsistency in material output. Once the flow is consistent, the robot moves to the crack coordinates and begins the filling process.

As the robot follows the optimized path along the crack, the extruder deposits the material precisely into the crack. Throughout the process, the robot speed is adjusted based on each crack coordinates' cross-sectional area. The larger the area, the slower the robot and vice versa. This ensures that the crack is filled efficiently and effectively, enhancing the durability and longevity of the repair.

## 2.5 Validation

After the crack filling process is completed, the laser scanner is used again to perform a post-fill scan of the repaired crack. The same heuristic algorithm used during the initial scanning and calibration processes is applied to the post-fill scan data to detect the width and depth or height of the filled crack. An under-filled point will have some depth, while an over-filled point will have some height. The pre-fill and post-fill profiles are compared to assess the effectiveness of the repair. The absolute normalized difference between the pre-fill and post-fill profiles is calculated to quantify the accuracy of the repair, as shown in Eq. (11). Here,  $A_{pre}$  represents the cross-sectional area of the crack before filling, while  $A_{post}$  represents the cross-sectional area of the filled crack at the exact same coordinate. A lower value means a more accurate and effective repair, demonstrating a surface close to flat. By following this validation process, we ensure that the repairs meet the desired quality standards, providing a reliable and efficient approach to automated crack repair. The fill error,  $\epsilon_{fill}$  is given by.

$$\epsilon_{fill} = \left| \frac{A_{post}}{A_{pre}} \right| \quad (11)$$

## 3. Simulation and Experimental Setup

To evaluate the performance and validate the functionality of our automated crack repair system, we employed both simulation and experimental setups. The simulation environment allowed us to test and refine the system in a controlled virtual setting, minimizing potential issues before real-world deployment. The experimental setup provided a realistic testing environment to ensure the system's practical applicability and effectiveness.

### 3.1 Simulation Setup using RoboDK

The simulation environment used in this project is RoboDK, chosen for its robust robot Python programming API, cost-effectiveness, and ease of integration with real robots [47]. Fig. 7 shows the RoboDK simulation environment with the robot and end-effector as well as the simulated view from the camera. Using the robot's Python API, we can simulate the robot's motion both in the virtual environment and in the real world. RoboDK also has the capability to simulate a camera, allowing us to debug the crack detection and automation of robot motion. Both the real RGB-D camera and the laser scanner have their own Python APIs, facilitating smooth integration and implementation of all components in the real world. This comprehensive simulation setup ensures that we can thoroughly test and validate the system's functionality before deploying it in a real-world scenario, thereby minimizing potential issues and optimizing performance.

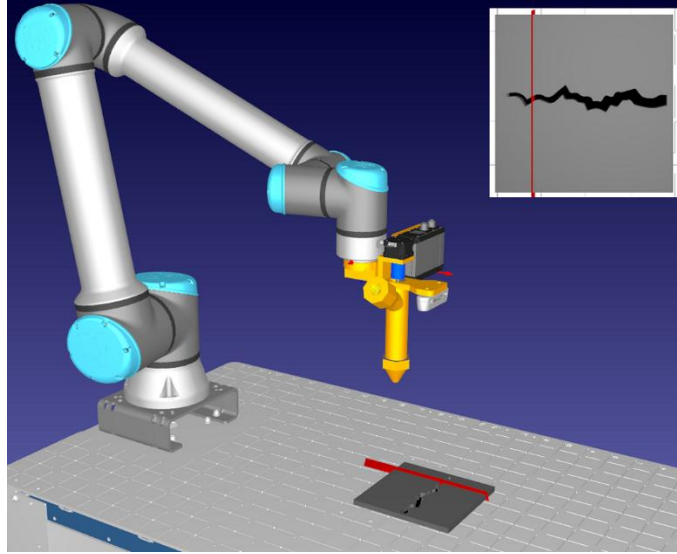


**Fig. 7.** RoboDK Simulation Environment.

## **3.2 Experimental Setup**

The experimental setup involves the physical implementation of the automated crack repair system. This section details the complete system design, covering various components essential for the repair process. We will explore the design and functionality of the end-effector, which is crucial for material extrusion. Then, we provide a detailed overview of the pump design, underlining its integration with the overall system. Finally, we discuss the 3D-printed crack specimens and the filling material used in the experiments, emphasizing their role in testing and validation.

### **3.2.1 System Design**

The whole system design integrates various components essential for the automated crack repair process. [Fig. 8](#) illustrates the complete setup, showcasing the interaction between the Universal Robot's UR10e robotic arm, end-effector, pump, microprocessor, and 3D-printed crack specimen. The UR10e robotic arm navigates along the crack and performs the repair with precision and a versatile reach, following the optimized path to deposit the repair material accurately. The print head, part of the end-effector, extrudes the filling material precisely into the crack, connected to the pump via tubing to ensure a steady flow. The custom-designed pump delivers the repair material from the reservoir to the print head, controlled by a microprocessor and motor drivers to maintain accurate flow rates. These microprocessor and motor drivers manage the pump and extruder operations, controlling the constant flow of material. The 3D-printed crack specimen mimics real-world crack patterns, allowing for effective testing and validation of the repair process. This integrated design facilitates efficient and accurate crack repair, demonstrating the potential of the automated system in real-world applications.

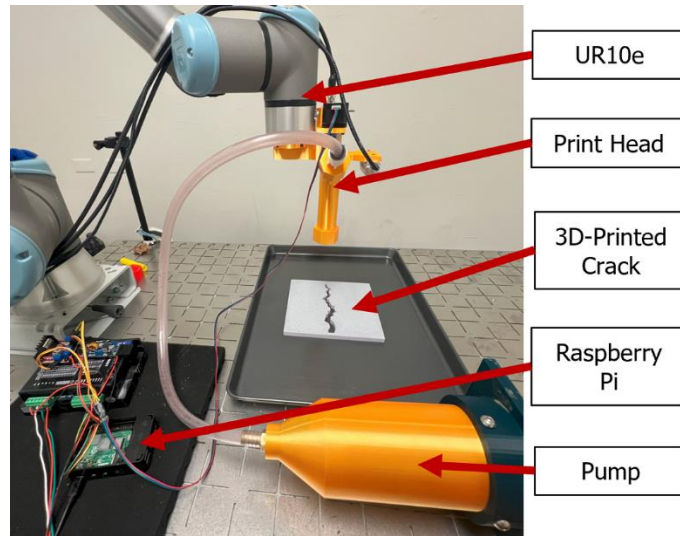


**Fig. 8.** System Design.

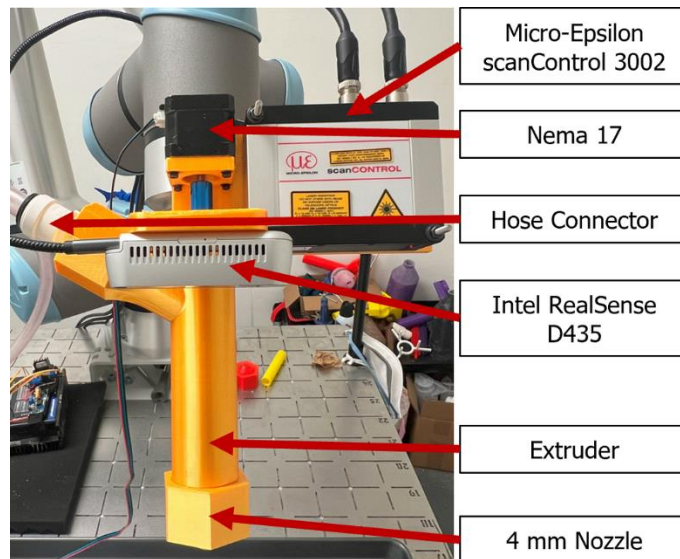


**Fig. 9.** End-Effector Design.

### 3.2.2 End-Effector Design

The end-effector is a crucial component of the automated crack repair system, designed to dispense the repair material precisely into the crack. Fig. 9 showcases the custom-designed end-effector, which includes key components such as the Intel RealSense D435 RGB-D camera, Micro-Epsilon scanCONTROL 3002 laser scanner, and the print head. The RGB-D camera captures images of the crack, offering an RGB image resolution of 1920x1080 with a field of view of 69° x 42° and a depth range of 0.3-3 m with an error margin of 2%. The laser scanner enhances robot coordinates and creates detailed crack profiles, featuring a measurement range of 200-420 mm in the z-axis, a resolution of 1024 points per profile, and a profile frequency of up to 10,000 Hz. The print head manages the material flow, delivered through flexible tubing to ensure consistent extrusion. The Nema 17 stepper motor drives an auger inside the print head, rotating to extrude the material through the 4 mm nozzle. This custom-designed end-effector ensures that the repair

material is applied accurately and efficiently, contributing to the overall effectiveness and reliability of the crack repair system.

### **3.2.3 Pump Design**

The pump system is designed to deliver material to the print head efficiently. It comprises 3D printed parts, a Nema 34 stepper motor, O-rings, barbed hose, and a threaded rod. The pump's design is heavily influenced by the structure of a medical syringe, featuring a cylinder-to-cone shape and a plunger mechanism that facilitates the extrusion of material from the pump to the hose and ultimately to the print head. The motor's movement, whether extending or retracting, controls the threaded rod, which in turn moves the piston. When the motor extends, the piston pushes the material inside the pump through the nozzle of the extruder via the tube. The efficiency of the pump is influenced by the diameter of the barbed hose and the viscosity of the material. A larger hose diameter and less viscous material typically results in a higher success rate of extrusion and flow. To improve the pump's performance, several modifications were made. The infill of the 3D printed pump was increased to enhance its structural integrity. Tolerances for the O-rings were minimized to prevent leakage, ensuring a reliable seal. Adjustments were made to handle different viscosities and types of materials, enhancing versatility. The design was refined to ensure the pump is safe and easy to use. Efforts were made to minimize material waste and enhance the overall efficiency of the extrusion process. These changes have collectively increased the pump's efficiency, durability, and user-friendliness, resulting in a more consistent extrusion system with minimal material waste.

### **3.2.4 3D-Printed Crack and Filling Material**

To test and validate the automated crack repair system, we used 3D-printed crack specimens that mimic real-world crack patterns. These specimens are designed to represent various crack widths, depths, and orientations, providing a robust testing environment for the repair process. The crack specimens are created using a high-resolution 3D printer, ensuring precise replication of different crack geometries. Play Doh mixed with water is used as the filling material due to its ease of testing and reusability. This mixture can be replaced with other materials by simply repeating the calibration setup. The 3D-printed crack specimens are then placed in the testing area, where the robotic system applies the filling material according to the programmed repair procedure.

## **4. Results**

This section presents the results of our automated crack repair system, focusing on the calibration and validation processes. The calibration results demonstrate the relationship between the robot's speed and material extrusion rate, essential for ensuring optimal material flow during repairs. The validation results assess the accuracy of the crack filling process, comparing pre-fill and post-fill profiles to evaluate the system's effectiveness. In addition, a video link demonstrating the whole crack filling process can be found [here](#).

### **4.1 Calibration Results**

Accurate material extrusion during crack repair relies heavily on a precise calibration process. To begin, we print a material strip 150 mm in length at a constant robot speed and flow rate. We then use the laser scanner to scan the inner 100 mm of the strip, as the extrusion may be inconsistent at the beginning and at the end of the print. By scanning the middle portion in 10 mm increments, we determine the average cross-sectional area using the heuristic approach discussed previously. Fig. 10 shows a graph of the print or crack profile where the green and violet circles indicate the indices of the largest sudden change, and the red circle is the center. This process is repeated at different robot speeds to measure the amount of material extruded at each speed, as illustrated in Fig. 11.

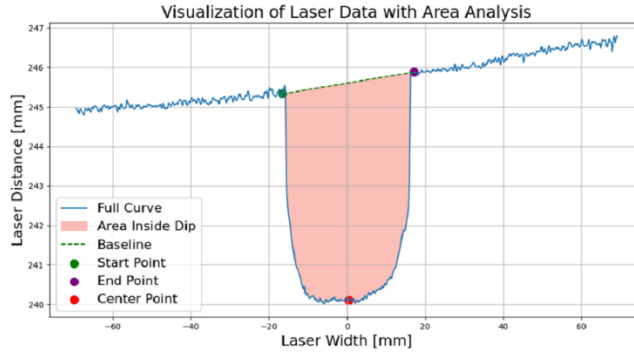


**Fig. 10.** Sample Profile of Calibration Print.

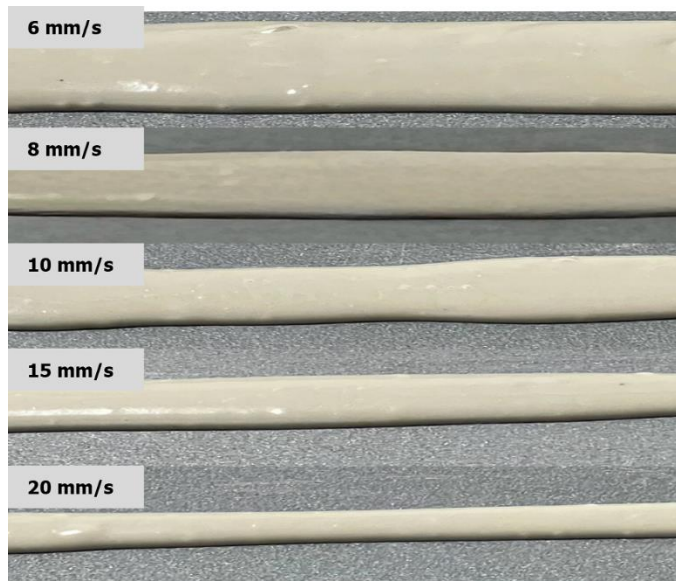


**Fig. 11.** Material Extrusion at Different Robot Speeds.

The calibration process aimed to determine the relationship between the robot's speed and the amount of material extruded. Various speeds were tested, and the cross-sectional areas of the extruded material were measured. The results, summarized in Table 1, show a clear inverse relationship between the robot's speed and the material extrusion rate: as the robot's speed increases, the amount of material extruded decreases, and vice versa. This calibration allows us to associate specific speeds with their corresponding cross-sectional areas, which is essential for the crack filling process. Each crack coordinate, having varying sizes, requires an appropriate speed for optimal material extrusion.

**Table 1**  
Robot Speed vs. Cross Sectional Area

Robot Speed (mm/s)	Cross-Sectional Area (mm)	Std. Dev. (mm)
6	165.764	18.44
8	111.977	10.807
10	91.448	8.111
15	63.561	7.003
20	41.713	7.936

**Table 2**  
 $\epsilon_{fill}$  vs. Speed

Speed (mm/s)	Mean <sup>1</sup>	Std. Dev.	Median	Time (s)
6	2.499	3.682	1.186	39.844
8	1.63	2.753	0.387	31.333
10	1.175	2.497	0.221	28.000
15	0.448	0.555	0.265	21.944
20	0.711	0.568	0.608	19.102
<b>Adaptive</b>	<b>0.305</b>	<b>0.240</b>	<b>0.265</b>	<b>24.784</b>

<sup>1</sup>Mean refers to the average from 32 crack coordinates of their  $\epsilon_{fill}$

#### 4.2 Crack Filling Efficiency

The accuracy of the crack filling process was evaluated by comparing the pre-fill and post-fill profiles as described in Eq. (11). Table 2 presents the error values  $\epsilon_{fill}$  for various constant speeds, including adaptive speed control. The results indicate that adaptive speed control achieved the lowest error or highest accuracy, with a mean  $\epsilon_{fill}$  of 0.305, a standard deviation of 0.240, and a median of 0.265. In comparison, fixed speeds of 6 mm/s, 8 mm/s, 10 mm/s, 15 mm/s, and 20 mm/s resulted in higher mean and standard deviation values, pointing out less precise filling with a higher degree of overfill or underfill. Fig. 12 demonstrates the qualitative performance of different robot speeds during crack filling, where the adaptive speed shows the least amount of overfill and underfill. Fig. 13 also shows the graph overlay of the crack profile at pre-fill vs. post-fill, which shows the adaptive speed with minimal underfill and overfill. At speed 6 mm/s, there is a large amount of overfill and at speed 20 mm/s, there is a large amount of underfill which is apparent in both Fig. 12. and Fig. 13. The repair process time also varied with speed, with adaptive speed control completing the process in 24.784 seconds, compared to 39.844 seconds for the 6 mm/s speed and 19.102 seconds for the 20 mm/s speed. While the 20 mm/s speed resulted in the shortest repair time, it bargained the filling accuracy, leading to higher deviations in the filled profiles. On the other hand, the adaptive speed control not only provided the most accurate filling but also optimized the repair time by balancing speed and precision. These findings confirm that the automated crack repair system, applying adaptive speed control, can effectively adjust the material flow based on robot speed and deposition based on crack profile data, ensuring accurate and consistent repairs.

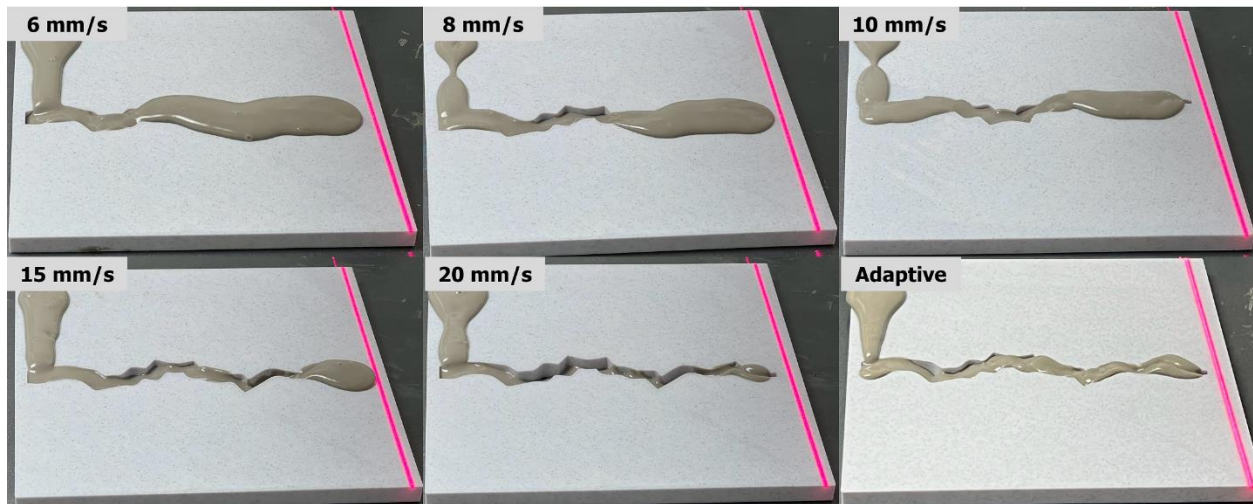


**Fig. 12.** Filled Crack with Different Speeds.

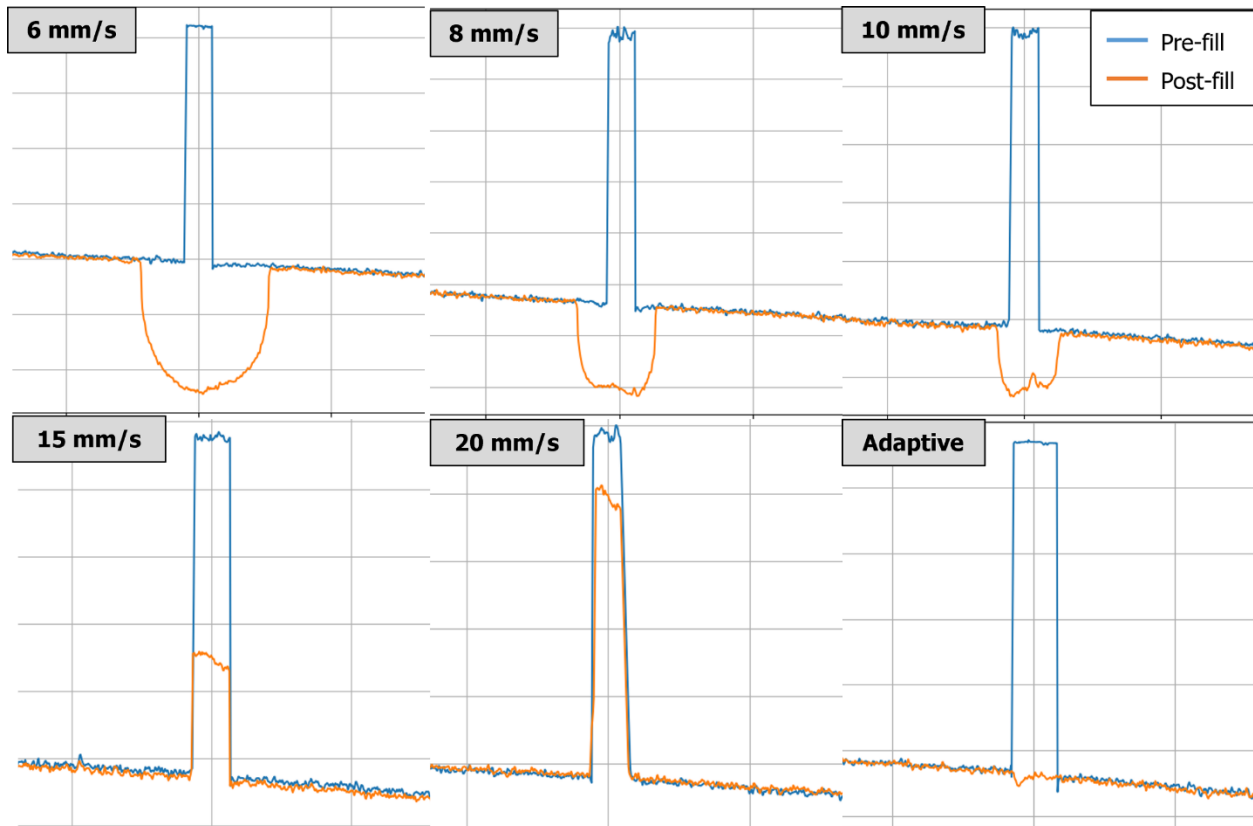


**Fig. 13.** Visual Overlay of Pre-Fill vs. Post-Fill.

## 5. Conclusion

This paper presented a novel design for an adaptive, autonomous system for surface crack detection and repair using a robotic arm equipped with advanced sensing technologies. The system integrates an RGB-D camera for initial crack detection, a laser scanner for precise measurement and profile generation, and an extruder for material deposition. To enable an adaptive repair that significantly enhances repair precision and efficiency, our approach first automatically calibrates the relationship between the robot's speed and material extrusion rate. Then, the system is able to utilize precise crack perception to ensure optimal material flow for varying crack sizes. Additionally, a novel and repeatable validation approach using a 3D-printed crack was developed. With the novel system design and validation approach, our study clearly demonstrates the benefits of an adaptive system for more efficient and effective filling of cracks compared to a fixed-speed filling. The experimental results confirmed the proposed system's capability to perform crack repairs effectively balancing the trade-off between repair time and filling precision. The use of 3D-printed crack specimens and a specially formulated filling material provided a robust and repeatable testing environment, closely simulating real-world conditions. The post-fill validation process, involving laser scanning and fill error calculation, highlighted the system's effectiveness in achieving accurate repairs. This research highlights the potential for adaptive, autonomous systems to significantly improve the quality and efficiency of infrastructure repair maintenance. Autonomous crack repair has the potential for widespread adoption across various infrastructure sectors ranging from residential, commercial, and transportation infrastructure, leading to enhanced safety, reduced maintenance costs, and extended lifespan of critical structures. By minimizing the need for manual labor, this approach not only improves worker safety but also meets the growing demand for automated solutions in infrastructure repair and maintenance.

## Author contributions: CRediT

**Joshua Genova:** Conceptualization, Formal analysis, Investigation, Methodology, Software, Validation, Visualization, Writing – original draft, Writing – review & editing. **Eric Cabera:** Investigation, Methodology, Writing - original draft. **Vedhus Hoskere:** Funding acquisition, Conceptualization, Project administration, Resources, Supervision, Visualization, Writing - original draft, Writing – review & editing

## Declaration of Competing Interest

The authors declare that they have no known competing financial interests or personal relationships that could have appeared to influence the work reported in this paper.

## Data availability

Data will be made available on request.

## Acknowledgements

The authors acknowledge partial financial support from the Department of Defense (Project No. G0511607). The contents of this paper reflect the views of the authors, who are responsible for the facts and the accuracy of the data presented herein. The contents do not necessarily reflect the official views or policies of the sponsors. The authors acknowledge the use of the Carya Cluster and the advanced support from the Research Computing Data Core at the University of Houston to carry out the research presented here.

## *Declaration of Generative AI and AI-assisted technologies in the writing process*

During the preparation of this work the authors used ChatGPT in order to improve readability and language. After using this tool, the authors reviewed and edited the content as needed and take full responsibility for the content of the publication.

## References

- [1] S. Stock, K. Nious, J. Carroll, M. Horn, Sinking, Pooling, Cracking: Runway Problems at San Francisco International Airport Cause More Delays for Travelers, NBC Bay Area (2019).
- [2] S. Khakurel, T.Z. Yeow, S.K. Saha, R.P. Dhakal, Post-Earthquake Building Assessment: How long do they take? Bulletin of the New Zealand Society for Earthquake Engineering 56 (2023) 115–126. <https://doi.org/10.5459/bnzsee.1568>.
- [3] S. Sattar, Recommended Options for Improving the Built Environment for Post-Earthquake Reoccupancy and Functional Recovery Time, Gaithersburg, MD, 2021. <https://doi.org/10.6028/NIST.SP.1254>.
- [4] F. Gong, X. Cheng, B. Fang, C. Cheng, Y. Liu, Z. You, Prospect of 3D printing technologies in maintenance of asphalt pavement cracks and potholes, J Clean Prod 397 (2023). <https://doi.org/10.1016/j.jclepro.2023.136551>.
- [5] V. Hoskere, Developing Autonomy in Structural Inspections through Computer Visions and Graphics, University of Illinois at Urbana-Champaign, 2020. <https://www.ideals.illinois.edu/items/117278> (accessed July 20, 2024).
- [6] B.F. Spencer, V. Hoskere, Y. Narazaki, Advances in Computer Vision-Based Civil Infrastructure Inspection and Monitoring, Engineering 5 (2019) 199–222. <https://doi.org/10.1016/j.eng.2018.11.030>.

- [7] Z. Yu, Y. Shen, Y. Zhang, Y. Xiang, Automatic crack detection and 3D reconstruction of structural appearance using underwater wall-climbing robot, *Automation in Construction* 160 (2024). <https://doi.org/10.1016/j.autcon.2024.105322>.
- [8] J.G. Victores, S. Martínez, A. Jardón, C. Balaguer, Robot-aided tunnel inspection and maintenance system by vision and proximity sensor integration, *Automation in Construction* 20 (2011) 629–636. <https://doi.org/10.1016/j.autcon.2010.12.005>.
- [9] B. Sutter, A. Lelevé, M.T. Pham, O. Gouin, N. Jupille, M. Kuhn, P. Lulé, P. Michaud, P. Rémy, A semi-autonomous mobile robot for bridge inspection, *Automation in Construction* 91 (2018) 111–119. <https://doi.org/10.1016/j.autcon.2018.02.013>.
- [10] M. Kouzehgar, Y. Krishnasamy Tamilselvam, M. Vega Heredia, M. Rajesh Elara, Self-reconfigurable façade-cleaning robot equipped with deep-learning-based crack detection based on convolutional neural networks, *Automation in Construction* 108 (2019). <https://doi.org/10.1016/j.autcon.2019.102959>.
- [11] K. Asadi, H. Ramshankar, H. Pullagurla, A. Bhandare, S. Shanbhag, P. Mehta, S. Kundu, K. Han, E. Lobaton, T. Wu, Vision-based integrated mobile robotic system for real-time applications in construction, *Automation in Construction* 96 (2018) 470–482. <https://doi.org/10.1016/j.autcon.2018.10.009>.
- [12] Y. Tian, C. Chen, K. Sagoe-Crentsil, J. Zhang, W. Duan, Intelligent robotic systems for structural health monitoring: Applications and future trends, *Automation in Construction* 139 (2022). <https://doi.org/10.1016/j.autcon.2022.104273>.
- [13] V. Hoskere, Y. Narazaki, T.A. Hoang, B.F. Spencer, MaDnet: multi-task semantic segmentation of multiple types of structural materials and damage in images of civil infrastructure, *Journal of Civil Structural Health Monitoring* 10 (2020) 757–773. <https://doi.org/10.1007/s13349-020-00409-0>.
- [14] Q.G. Alexander, V. Hoskere, Y. Narazaki, A. Maxwell, B.F. Spencer, Fusion of thermal and RGB images for automated deep learning based crack detection in civil infrastructure, *AI in Civil Engineering* 1 (2022). <https://doi.org/10.1007/s43503-022-00002-y>.
- [15] J. Wang, Z. Zeng, P.K. Sharma, O. Alfarraj, A. Tolba, J. Zhang, L. Wang, Dual-path network combining CNN and transformer for pavement crack segmentation, *Automation in Construction* 158 (2024). <https://doi.org/10.1016/j.autcon.2023.105217>.
- [16] M.A.M. Khan, R.W. Harseno, S.H. Kee, A. Al Nahid, Development of AI- and Robotics-Assisted Automated Pavement-Crack-Evaluation System, *Remote Sensing* 15 (2023). <https://doi.org/10.3390/rs15143573>.
- [17] K. Hunte, Motion Planning and Control of an Automated Crack Filling Robot for Unknown Environments, Rutgers, The State University of New Jersey, 2023.
- [18] A. Ghadimzadeh Alamdari, A. Ebrahimkhanlou, A multi-scale robotic approach for precise crack measurement in concrete structures, *Automation in Construction* 158 (2024). <https://doi.org/10.1016/j.autcon.2023.105215>.
- [19] K. Hu, Z. Chen, H. Kang, Y. Tang, 3D vision technologies for a self-developed structural external crack damage recognition robot, *Automation in Construction* 159 (2024). <https://doi.org/10.1016/j.autcon.2023.105262>.
- [20] M. Stevens, S. Arellano, D. Rodriguez, J. Wilson New Mexico Tech, N. Zady Gutierrez, N. Trudell, H. Momeni, A. Ebrahimkhanlou, Robotic-based Repair of Concrete Structures: A surface crack filler robot, 2021. <http://asmedigitalcollection.asme.org/IMECE/proceedings-pdf/IMECE2021/85697/V013T15A014/6829312/v013t15a014-imece2021-72082.pdf>.
- [21] L. Wunsch, C.G. Tenorio, K. Anding, A. Golomo, G. Notni, Data Fusion of RGB and Depth Data with Image Enhancement, *Journal of Imaging* 10 (2024). <https://doi.org/10.3390/jimaging10030073>.
- [22] J.C.H. Ong, M. Yoon, H. Shin, S.-E. Yoon, Z. Pan, M.-Z. Ismadi, X. Wang, Metaheuristic Crack Sealing Path Planning based on Discrete Grey Wolf Optimizer, n.d. <https://ssrn.com/abstract=4684040>.

- [23] Z. Li, Y. Miao, M.E. Torbaghan, H. Zhang, J. Zhang, Semi-automatic crack width measurement using an OrthoBoundary algorithm, *Automation in Construction* 158 (2024). <https://doi.org/10.1016/j.autcon.2023.105251>.
- [24] J.M. Sáez-López, M.L. Sevillano-García, E. Vazquez-Cano, The effect of programming on primary school students' mathematical and scientific understanding: educational use of mBot, *Educational Technology Research and Development* 67 (2019) 1405–1425. <https://doi.org/10.1007/s11423-019-09648-5>.
- [25] A. Sheta, S.A. Mokhtar, Autonomous Robot System for Pavement Crack Inspection Based CNN Model, *Journal of Theoretical and Applied Information Technology* 31 (2022). [www.jatit.org](http://www.jatit.org).
- [26] F. Xu, S. Dai, Q. Jiang, X. Wang, Developing a climbing robot for repairing cables of cable-stayed bridges, *Automation in Construction* 129 (2021). <https://doi.org/10.1016/j.autcon.2021.103807>.
- [27] T.H. Lin, C.T. Chang, B.H. Yang, C.C. Hung, K.W. Wen, AI-powered shotcrete robot for enhancing structural integrity using ultra-high performance concrete and visual recognition, *Automation in Construction* 155 (2023). <https://doi.org/10.1016/j.autcon.2023.105038>.
- [28] R. Chen, C. Zhou, L. Cheng, Computer-vision-guided semi-autonomous concrete crack repair for infrastructure maintenance using a robotic arm, *AI in Civil Engineering* 1 (2022). <https://doi.org/10.1007/s43503-022-00007-7>.
- [29] G. Zhu, Z. Fan, W. Chen, Y. You, S. Huang, W. Liang, R. Fu, J. Xin, J. Chen, F. Deng, Y. Hou, Design and Implementation of a Manipulator System for Roadway Crack Sealing, in: 2019 IEEE 9th Annual International Conference on CYBER Technology in Automation, Control, and Intelligent Systems (CYBER), IEEE, Suzhou, China, 2019: pp. 1327–1331. <https://doi.org/10.1109/CYBER46603.2019.9066587>.
- [30] K. Yu, C. Guo, J. Yi, Complete and Near-Optimal Path Planning for Simultaneous Sensor-Based Inspection and Footprint Coverage in Robotic Crack Filling, in: International Conference on Robotics and Automation (ICRA), IEEE Xplore, Montreal, QC, Canada, 2019: pp. 8812–8818. <https://doi.org/10.1109/ICRA.2019.8794407>.
- [31] J. Zhang, X. Yang, W. Wang, J. Guan, W. Liu, H. Wang, L. Ding, V.C.S. Lee, Cross-entropy-based adaptive fuzzy control for visual tracking of road cracks with unmanned mobile robot, *Computer-Aided Civil and Infrastructure Engineering* 39 (2024) 891–910. <https://doi.org/10.1111/mice.13108>.
- [32] X. Yang, M. Kahouadji, O. Lakhali, R. Merzouki, Integrated design of an aerial soft-continuum manipulator for predictive maintenance, *Frontiers in Robotics and AI* 9 (2022). <https://doi.org/10.3389/frobt.2022.980800>.
- [33] M. Kahouadji, O. Lakhali, X. Yang, A. Belarouci, R. Merzouki, System of Robotic Systems for Crack Predictive Maintenance, in: 2021 16th International System of Systems Engineering Conference, SoSE 2021, Institute of Electrical and Electronics Engineers Inc., 2021: pp. 197–202. <https://doi.org/10.1109/SOSE52739.2021.9497490>.
- [34] M.E. Torbaghan, B. Kaddouh, M. Abdellatif, N. Metje, J. Liu, R. Jackson, C.D.F. Rogers, D.N. Chapman, R. Fuentes, M. Miodownik, R. Richardson, P. Purnell, Robotic and autonomous systems for road asset management: A position paper, *Proceedings of the Institution of Civil Engineers: Smart Infrastructure and Construction* 172 (2020) 83–93. <https://doi.org/10.1680/jsmic.19.00008>.
- [35] F.R. Pereira, C.D. Rodrigues, H. da S. e. Souza, J.O.C. Neto, M.C. Rocha, G.F. Barbosa, S.B. Shiki, R.S. Inoue, Force and vision-based system for robotic sealing monitoring, *International Journal of Advanced Manufacturing Technology* 126 (2023) 391–403. <https://doi.org/10.1007/s00170-023-11110-z>.
- [36] F.K.A. Awuah, A. Garcia-Hernández, Machine-filling of cracks in asphalt concrete, *Automation in Construction* 141 (2022). <https://doi.org/10.1016/j.autcon.2022.104463>.
- [37] M. Rahman, H. Liu, M. Rahimi, C.R. Carcel, L. Kirkwood, I.D. Cardenas, A. Starr, Investigating Precision and Accuracy of a Robotic Inspection and Repair System, 2021. <https://ssrn.com/abstract=3945943>.

- [38] S.D. Schaefer, J. Xu, D. Palin, A. Al-Tabbaa, F. Iida, Position-based fluid simulation for robotic injection sealing of pavement cracks, *Journal of Field Robotics* (2024). <https://doi.org/10.1002/rob.22339>.
- [39] E. Bianchi, M. Hebdon, Development of Extendable Open-Source Structural Inspection Datasets, *Journal of Computing in Civil Engineering* 36 (2022). [https://doi.org/10.1061/\(asce\)cp.1943-5487.0001045](https://doi.org/10.1061/(asce)cp.1943-5487.0001045).
- [40] F. Yang, L. Zhang, S. Yu, D. Prokhorov, X. Mei, H. Ling, Feature Pyramid and Hierarchical Boosting Network for Pavement Crack Detection, *IEEE Transactions on Intelligent Transportation Systems* 21 (2019) 1525–1535. <https://github.com/fyangneil/pavement-crack-detection>.
- [41] Y. Shi, L. Cui, Z. Qi, F. Meng, Z. Chen, Automatic road crack detection using random structured forests, *IEEE Transactions on Intelligent Transportation Systems* 17 (2016) 3434–3445. <https://doi.org/10.1109/TITS.2016.2552248>.
- [42] Q. Zou, Y. Cao, Q. Li, Q. Mao, S. Wang, CrackTree: Automatic crack detection from pavement images, *Pattern Recognition Letters* 33 (2012) 227–238. <https://doi.org/10.1016/j.patrec.2011.11.004>.
- [43] Y. Liu, J. Yao, X. Lu, R. Xie, L. Li, DeepCrack: A deep hierarchical feature learning architecture for crack segmentation, *Neurocomputing* 338 (2019) 139–153. <https://doi.org/10.1016/j.neucom.2019.01.036>.
- [44] M. Eisenbach, R. Stricker, D. Seichter, K. Amende, K. Debes, M. Sesselmann, D. Ebersbach, U. Stoeckert, H.-M. Gross, How to get pavement distress detection ready for deep learning? A systematic approach, in: *2017 International Joint Conference on Neural Networks (IJCNN)*, IEEE, Anchorage, AK, USA, 2017: pp. 2039–2047. <https://doi.org/10.1109/IJCNN.2017.7966101>.
- [45] X. Weng, Y. Huang, W. Wang, Segment-based pavement crack quantification, *Autom Constr* 105 (2019). <https://doi.org/10.1016/j.autcon.2019.04.014>.
- [46] N. Van Oosterwyck, Real Time Human Robot Interactions and Speed Control of a Robotic Arm for Collaborative Operations, (2018). <https://doi.org/10.13140/RG.2.2.28723.53286>.
- [47] RoboDK Inc., RoboDK, (2024).